# A simulation of the large-scale drifting snow storm in a turbulent boundary layer

**Zhengshi Wang[1,2], Shuming Jia [1,2*]**

[1] State Key Laboratory of Aerodynamics, China Aerodynamic Research and Development Center, Mianyang Sichuan 621000, China

[2] Computational Aerodynamics Institute, China Aerodynamics Research and Development Center, Mianyang, Sichuan 621000, China

[*] **Corresponding:** Shuming Jia (jiashm17@cardc.cn)

**Abstract.** Drifting snow storm is an important aeolian process that reshapes alpine glaciers and polar ice shelves, and it may also affect the climate system and hydrological cycle since flying snow particles exchange considerable mass and energy with air flow. Prior studies have rarely considered the full-scale drifting snow storm in the turbulent boundary layer, thus, the transportation feature of snow flow higher in the air and its contribution are largely unknown. In this study, a large eddy simulation is combined with a subgrid scale velocity model to simulate the atmospheric turbulent boundary layer, and a Lagrangian particle tracking method is adopted to track the trajectories of snow particles. A drifting snow storm that is hundreds of meters in depth and exhibits obvious spatial structures is produced. The snow transport flux profile at high altitude, previously not observed, is quite different from that near the surface, thus, the extrapolated transport flux profile may largely underestimate the total transport flux. At the same time, the development of a drifting snow storm involves three typical stages, the rapid growth, the gentle growth and the equilibrium stages, in which the large-scale updrafts and subgrid scale fluctuating velocities basically dominate the first and second stage, respectively. This research provides an effective way to get an insight into natural drifting snow storms.

# 1 Introduction

Snow, one type of solid precipitation, is an important sources of material to mountain glaciers and polar ice sheets, which are widespread throughout high and cold regions (Chang et al., 2016; Gordon and Taylor, 2009; Lehning et al., 2008). A common natural phenomenon over snow cover is the drifting snow storm, which occurs when the wind speed exceeds a critical value (Doorschot et al., 2004; Li and Pomeroy, 1997; Sturm and Stuefer, 2013). Drifting snow can entrain loose snow particles on the bed into the air, which may be further transported to high altitude by turbulent eddies (King, 1990; Mann et al., 2000; Nemoto and Nishimura, 2004). Drifting snow clouds typically can range in thickness from tens to thousands of meters (Mahesh et al., 2003; Palm et al., 2011), which may not only affect people's daily life by reducing the visibility and producing local accumulation (Gordon and Taylor, 2009; Mohamed et al., 1998) , but also can influence the global climate system evolution by changing the mass and energy balance of ice shelves (Cess and Yagai, 1991; Hanesiak and Wang, 2005; Hinzman et al., 2005; Lenaerts and Broeke, 2012).

Several field experiments on drifting snow storm have been performed (Bintanja, 2001; Budd, 1966; Dingle and Radok, 1961; Doorschot et al., 2004; Gallée et al., 2013; Gordon and Taylor, 2009; Guyomarch et al., 2014; Kobayashi, 1978; Mann et al., 2000; K Nishimura and Nemoto, 2005; Kouichi Nishimura et al., 2015; J. W. Pomeroy and Gray, 1990; Sbuhei, 1985; Schmidt, 1982; Sturm and Stuefer, 2013) since the middle of the last century. However, the measurements are commonly conducted near the surface, thus, the drifting snow features at high altitude are

unknown, and the impacts of these features are difficult to assess. A thorough investigation documenting the evolution process and structure of a full-scale drifting snow storm is essential to understand this natural phenomenon and assess its impacts.

Drifting snow models, on the other hand, offer a panoramic view of the evolution process of drifting snow and thus have become one of the most useful research approaches. Many continuum medium models of drifting snow (Bintanja, 2000; Déry and Yau, 1999; Schneiderbauer and Prokop, 2011; Uematsu et al., 1991; Vionnet et al., 2013) have advanced the knowledge of natural drifting snow to a great extent. However, a particle-tracking drifting snow model is still needed since the particle characteristics and its motion require further investigation. Although a series of particle tracking models (Huang et al., 2016; Huang and Shi, 2017; Huang and Wang, 2015; 2016; Nemoto and Nishimura, 2004; Zhang and Huang, 2008; Zwaaftink et al., 2014) have been established, these models have generally focused on the grain-bed interactions and particle motions near the surface. Thus, a drifting snow model aimed at producing a large-scale drifting snow storm in a turbulent boundary layer deserves further exploration.

In this study, a drifting snow model in the atmospheric boundary layer that focuses on the full-scale drifting snow storm is established. The wind field is solved using a large eddy simulation for the purpose of generating a turbulent atmospheric boundary layer. A subgrid scale (SGS) velocity is also considered to include the diffusive effect of small scale turbulence. Finally, particle motion is calculated using a Lagrangian particle tracking method. The large-scale drifting snow storm is produced under the

actions of large-scale turbulent structures combined with a steady-state snow saltation boundary condition for particles, and its spatial structures and transport features are analyzed.

# 2 Model and methods

## 2.1 Simulation of a turbulent atmospheric boundary layer

The mesoscale atmosphere prediction pattern ARPS (Advanced Regional Prediction System, version 5.3.3) is adopted to simulate the turbulent atmospheric boundary layer, in which the filtered three-dimensional compressible non-hydrostatic Naiver-Stokes equation is solved (Xue et al., 2001):

$$\frac{\partial \rho}{\partial t}+\frac{\partial}{\partial x_i}(\rho \tilde{u}_i)=0 \tag{1}$$

$$\frac{\partial \rho \tilde{u}_i}{\partial t}+\frac{\partial \rho u_i \tilde{u}_j}{\partial x_j}=-\frac{\partial \tilde{p}^*}{\partial x_i}+B\delta_{i3}-\frac{\partial \tau_{ij}}{\partial x_j} \tag{2}$$

where '~' represents variables that are filtered and the filtering scale is $\tilde{\Delta}=\left(\Delta x_1 \Delta x_2 \Delta x_3\right)^{1/3}$, in which $\Delta x_i$ is the grid spacing along streamwise ($i=1$), spanwise ($i=2$) and vertical direction ($i=3$), respectively. $\rho = p(1-q_v/(\varepsilon+q_v))(1+q_v)/(R_d T)$ is the air density, in which $p$, $q_v$, $R$ and $T$ are the pressure, the specific humidity, the gas constant (287.0 $Jkg^{-1}K^{-1}$) and temperature of the air, respectively, and $\varepsilon$=0.622 is a constant. $u_i$ is the instantaneous wind speed component, and $x_i$ is the position coordinate. $t$ is time, $\delta_{ij}$ is the Kronecker delta, $B=-g\rho'/\rho$ is the buoyancy caused by the air density perturbation $\rho'$, and $g$ is the acceleration due to gravity. $p^*=p'-\alpha\nabla(\rho\mathbf{u})$ contains the pressure perturbation term and damping term, where $\alpha=0.5$ is the damping

coefficient and $\nabla$ is the divergence. The subgrid stress $\tau_{ij}$ can be expressed as (Smagorinsky, 1963):

$$\tau_{ij} = -2\nu_t \tilde{S}_{ij} = -2\left(C_s\tilde{\Delta}\right)^2 \left|\tilde{S}\right|\tilde{S}_{ij} \tag{3}$$

where $\tilde{S}_{ij} = 0.5\left(\partial\tilde{u}_i/\partial x_j + \partial\tilde{u}_j/\partial x_i\right)$ is the strain rate tensor and $\left|\tilde{S}\right| = \sqrt{2\tilde{S}_{ij}\tilde{S}_{ij}}$, $C_s$ is Smagorinsky coefficient that is determined locally by the dynamic Lagrangian model (Meneveau et al., 1996).

~~Considering the large grid spacing in simulating an atmospheric boundary layer (where the information about turbulent vortices smaller than the grid size is missing), the SGS velocity is also included. Namely, the local wind velocity $\tilde{u}_i\left(\vec{x}(t)\right)$ is composed of a resolved Eulerian large-scale part $\tilde{u}_i\left(\vec{x}(t)\right)$ (obtained from the linear weighting of surrounding grid points) and a fluctuating SGS contribution $u_i'(t)$. The SGS velocity can be calculated from the SGS stochastic model of Vinkovic et al. (2006):~~

$$du_i' = -\left(\frac{1}{T_L} + \frac{1}{2\tilde{k}}\frac{d\tilde{k}}{dt}\right)u_i' dt + \sqrt{\frac{4\tilde{k}}{3T_L}}d\eta_i(t) \tag{4}$$

~~where $T_L = 4\tilde{k}/\left(3C_0\tilde{\varepsilon}\right)$ is the Lagrangian correlation time scale. Here, $C_0$ is the Lagrangian constant, $\tilde{\varepsilon} = C_\varepsilon\tilde{k}^{3/2}/\tilde{\Delta}$ is the subgrid turbulence dissipation rate, $C_\varepsilon$ is a constant, and $d\eta_i$ is the increment of a vector-valued Wiener process with zero mean and variance $dt$. $\tilde{k}$ is the subgrid turbulent kinetic energy and can be obtained from the transport equation (Deardorff, 1980):~~

$$\frac{\partial\tilde{k}}{\partial t} + \tilde{u}_j\frac{\partial\tilde{k}}{\partial x_j} = \frac{\nu_t}{3}\frac{g}{\theta_0}\frac{\partial\tilde{\theta}}{\partial x_3} + 2\nu_t\tilde{S}_{ij}^2 + 2\frac{\partial}{\partial x_j}\left(\nu_t\frac{\partial\tilde{k}}{\partial x_j}\right) + \tilde{\varepsilon} \tag{5}$$

~~where $\theta$ is the potential temperature and $\theta_0$ is the surface potential temperature.~~

## 2.2 Governing equation of particle motion

The trajectory of each snow particle is calculated using a Lagrangian particle tracking method. Since a snow particle has is almost $10^3$ times more dense than air, airborne particles are assumed to process only gravity and fluid drag forces, and the governing equations of particle motion can be expressed as (Dupont et al., 2013; Huang and Wang, 2016; Vinkovic et al., 2006):

$$\frac{dx_{pi}}{dt} = u_{pi} \tag{4}$$

$$\frac{du_{pi}}{dt} = m_p \frac{V_{ri}}{T_p} f(Re_p) + \delta_{i3} g \tag{5}$$

where $x_{pi}$ and $u_{pi}$ are the position coordinate and velocity of the snow particle, respectively. $m_p$ is the mass of the solid particle, $V_r$ is the relative speed between the snow particle and air, and $T_p = \rho_p d_p^2 / 18\rho\nu$ is the particle relaxation time, where $\rho_p$ is the particle density (900 $kgm^{-3}$), $d_p$ is the particle diameter and $\nu = 1.5e-5$ is the dynamic viscosity of air. $f\left(Re_p\right)$ can be expressed as (Clift et al., 1978):

$$f(Re_p) = \begin{cases} 1 & (Re_p < 1) \\ 1 + 0.15\,\mathrm{Re}_p^{0.687} & (Re_p \geq 1) \end{cases} \tag{6}$$

where $Re_p = V_r d / \nu$ is the particle Reynolds number.

Considering the large grid spacing in simulating an atmospheric boundary layer (where the information about turbulent vortices smaller than the grid size is missing), the SGS velocity is also included and attached on the particle. Namely, the local relative is expressed as $V_{ri} = \tilde{u}_i\left(x_p\right) - u_{pi} + u_i'$, in which $\tilde{u}_i\left(\vec{x}_p\right)$ is the resolved large-scale wind speed at the particle's position and is determined by the resolved wind speeds of surrounding grid points through the linear interpolation algorithm. The

SGS velocity can be calculated from the SGS stochastic model of Vinkovic et al. (2006):

$$du_i' = \left( -\frac{1}{T_L} + \frac{1}{2\tilde{k}} \frac{d\tilde{k}}{dt} \right) u_i' dt + \sqrt{\frac{4\tilde{k}}{3T_L}} d\eta_i(t) \quad (7)$$

where $T_L = 4\tilde{k} / (3C_0\tilde{\varepsilon})$ is the Lagrangian correlation time scale. Here, $C_0 = 2.1$ is the Lagrangian constant, $\tilde{\varepsilon} = C_\varepsilon \tilde{k}^{3/2} / \tilde{\Delta}$ is the subgrid turbulence dissipation rate, $C_\varepsilon = 0.41$ is a constant, and $d\eta_i$ is the increment of a vector-valued Wiener process with zero mean and variance $dt$. $\tilde{k}$ is the subgrid turbulent kinetic energy and can be obtained from the transport equation (Deardorff, 1980):

$$\frac{\partial \tilde{k}}{\partial t} + \tilde{u}_j \frac{\partial \tilde{k}}{\partial x_j} = \frac{\nu_t}{3} \frac{g}{\theta_0} \frac{\partial \tilde{\theta}}{\partial x_3} + 2\nu_t \tilde{S}_{ij}^2 + 2 \frac{\partial}{\partial x_j} \left( \nu_t \frac{\partial \tilde{k}}{\partial x_j} \right) + \tilde{\varepsilon} \quad (8)$$

where $\theta$ is the potential temperature and $\theta_0$ is the surface potential temperature.

### 2.3 Initial conditions of snow particles

To generate a large-scale drifting snow storm, a steady-state snow saltation condition is set as the bottom boundary condition for particles. During drifting snow events, the sum of residual fluid shear stress $\tau_f$ and particle-borne shear stress $\tau_p$ should be equal to the total ~~fluid~~ shear stress $\tau$, thus, the particle-borne stress can be expressed as:

$$\tau_p = \tau - \tau_f \quad (9)$$

Here, the residual fluid shear stress $\tau_f$ is set to be the threshold shear stress $\tau_{tf}$ of drifting snow, which can be read as (Clifton et al., 2006):

$$\tau_{tf} = A^2 g d \left( \rho_p - \rho \right) \quad (10)$$

in which $A = 0.2$ is a constant, $g$ is the gravity acceleration and $d$ is the mean

diameter of the snow particles.

At the same time, the particle-borne shear stress at the surface can be calculated from the particle trajectories as (Nemoto and Nishimura, 2004):

$$\tau_p = \sum_{i=1}^{n_\downarrow} m_i u_{pi\downarrow} - \sum_{i=1}^{n_\uparrow} m_i u_{pi\uparrow} \tag{11}$$

where $m_i$ is the mass of particle and $u_{pi\downarrow}$ and $u_{pi\uparrow}$ are the horizontal speeds of impact and lift-off particles, respectively. $n_\downarrow$ and $n_\uparrow$ are the particle number per unit area in unit time of impact and lift-off grains, respectively, which should be equivalent in steady-state saltation. Thus, the number of lift-off particles per unit area is:

$$n_\uparrow = n_\downarrow = \frac{\tau_p}{\langle m_i \rangle \left(1 - \langle e_h \rangle\right) \langle u_{pi\downarrow} \rangle} \tag{12}$$

in which $\langle\ \rangle$ indicates the overall average, and $e_h$ is the horizontal restitution coefficient of snow particle. According to Sugiura and Maeno (2000), the mean horizontal restitution coefficient can be expressed as:

$$\langle e_h \rangle = \begin{cases} 0.48\theta_i^{0.01} & v_i \le 1.27 ms^{-1} \\ 0.48\left(\dfrac{v_i}{1.27}\right)^{-\log\left(\frac{v_i}{1.27}\right)} \theta_i^{0.01} & v_i > 1.27 ms^{-1} \end{cases} \tag{13}$$

where $\theta_i$ and $v_i$ are the impact velocity and angle, respectively. Here, $\theta_i$ has a mean value of approximately 10° (Sugiura and Maeno, 2000), and $\langle v_i \rangle$ is set to be the threshold of impact velocity~~,~~. Considering the steady-state saltation condition (one impact particle generates one ejecta on average), $\langle v_i \rangle$ ~~which~~ is determined by setting ejection number $n_e = 0.51 v_i^{0.6} \theta_i^{0.16}$ equal to 1. In this way, the mean horizontal

velocity of impact particles can be obtained through $\left\langle u_{pi\downarrow} \right\rangle = \left\langle v_i \right\rangle \cos\left\langle \theta_i \right\rangle$.

Then, the velocities of lift-off particles can be obtained from the restitution coefficient of snow. The horizontal restitution coefficient obeys the normal distribution with a mean value given in Eq. 13, and a standard variance as follow (Sugiura and Maeno, 2000):

$$\sigma^2 = \begin{cases} 0.07\theta_i^{-0.06} & v_i \le 0.52\ ms^{-1} \\ 0.07\left(\dfrac{v_i}{0.52}\right)^{-\log\left(\frac{v_i}{0.52}\right)} \theta_i^{-0.06} & v_i > 0.52\ ms^{-1} \end{cases} \tag{14}$$

On the other hand, the vertical restitution coefficient can be described by a two parameter gamma function (see Eq. 17), in which the parameter $\alpha$ and $\beta$ can be expressed as (Sugiura and Maeno, 2000):

$$\alpha = \begin{cases} 1.22\theta_i^{0.47} & v_i \ge 0.84\ ms^{-1} \\ 1.22\left(\dfrac{v_i}{0.84}\right)^{\log\left(\frac{v_i}{0.84}\right)} \theta_i^{0.47} & 0.84 < v_i \le 1.23\ ms^{-1} \\ 1.22\left(\dfrac{v_i}{0.84}\right)^{\log\left(\frac{v_i}{0.84}\right)} \left(\dfrac{v_i}{1.23}\right)^{-2\log\left(\frac{v_i}{1.23}\right)} \theta_i^{0.47} & v_i \ge 1.23\ ms^{-1} \end{cases} \tag{15}$$

$$\beta = \begin{cases} 12.85\theta_i^{-1.41} & v_i \ge 0.84\ ms^{-1} \\ 12.85\left(\dfrac{v_i}{0.84}\right)^{-\log\left(\frac{v_i}{0.84}\right)} \theta_i^{-1.41} & 0.84 < v_i \le 1.23\ ms^{-1} \\ 12.85\left(\dfrac{v_i}{0.84}\right)^{-\log\left(\frac{v_i}{0.84}\right)} \left(\dfrac{v_i}{1.23}\right)^{\log\left(\frac{v_i}{1.23}\right)} \theta_i^{-1.41} & v_i \ge 1.23\ ms^{-1} \end{cases} \tag{16}$$

In this condition, if some of the snow particles within the saltation layer are transported to higher in the air by turbulent vortexes (the saltation layer becomes undersaturated), more particles will lift-off from the surface to replenish the saltation layer until a saturated state is reached.

## 2.4 Simulation details

189 The computational domain is 1000×500×1000 m, with a uniform horizontal grid
190 size of 5 m adopted to solve finer vortex structure in the atmospheric boundary layer.
191 The mean grid size in the vertical direction is 20 m, with a grid refinement algorithm
192 adopted near the surface (the finest grid size is 1 m). Periodic boundaries are used
193 along streamwise and spanwise dimensions, and the bottom is set as a grid wall. The
194 top is set as an open radiation boundary with a Rayleigh damping layer that is 250 m
195 in depth.

196 The atmosphere is neutral with an initial potential temperature of 300K, and an
197 initial relative humidity of 90%. The initial wind profile is logarithmic with a surface
198 roughness of 0.1m (Doorschot et al., 2004). Atmospheric turbulence is induced by
199 random initial potential temperature perturbations at the first-level grid level with a
200 maximum magnitude of 0.5K, and is sustained by a constant heat flux at the bottom.
201 The constant heat flux is 50 $Wm^{-2}$ according to the observation of Pomeroy and
202 Essery (1999). And the evolution time for a turbulent boundary layer is 5 times of the
203 large-eddy turnover time $t_*$ ($\equiv H/u_*$, where $H$ is the boundary layer depth and $u_*$
204 is the friction velocity). Actually, this condition corresponds to a 'intermediate'
205 turbulent boundary layer that dominated by wind shear force (Moeng and Sullivan,
206 1994). Thus, the structures of the drifting snow storm should not be affected by the
207 changing surface heat flux significantly if the surface heat flux is small. Further
208 simulations with different values of surface heat flux (<100 $Wm^{-2}$) also prove this
209 point.

210 For particles, periodic boundary conditions are also used at lateral boundaries, and

a rebound boundary condition without energy loss is adopted at the model top. The bottom boundary condition for particles is given in Sect. 2.3, and is updated every 0.5 s. Additionally, each particle represents one particle parcel for the purpose of reducing computational complexity. In this simulation, each particle parcel contains $10^7$ snow particles. The large time step and small time step (acoustic wave integral) for the wind field calculation are 0.1 s and 0.02 s, respectively, and the particle time step is determined by the minimum of particle relaxation time.

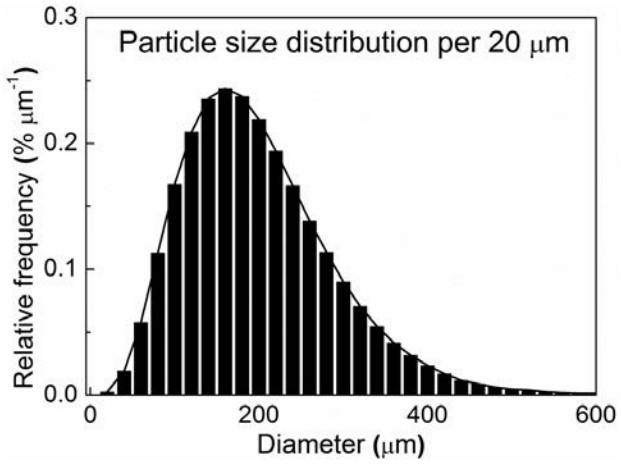


**Figure** 1. Size distribution of lift-off snow particles in this simulation.

The size distribution of lift-off particles in drifting snow can be well described by the two-parameter gamma function (Budd, 1966; Gordon and Taylor, 2009; Nishimura and Nemoto, 2005; Schmidt, 1982):

$$f(d) = \frac{d^{\alpha-1}}{\beta^{\alpha}\Gamma(\alpha)}\exp\left(-\frac{\beta}{d}\right) \tag{17}$$

where $d$ is the particle diameter, and $\alpha$ and $\beta$ are the shape and scale parameter of the distribution, respectively. In this simulation, the diameters of lift-off snow particles are given randomly from a gamma function with the parameters of $\alpha = 4$ and $\beta = 50$, as shown in Fig. 1, which is also consistent with observed particle size

distributions (Nishimura and Nemoto, 2005; Schmidt, 1982).

# 3 Results and discussions

## 3.1 Model validation

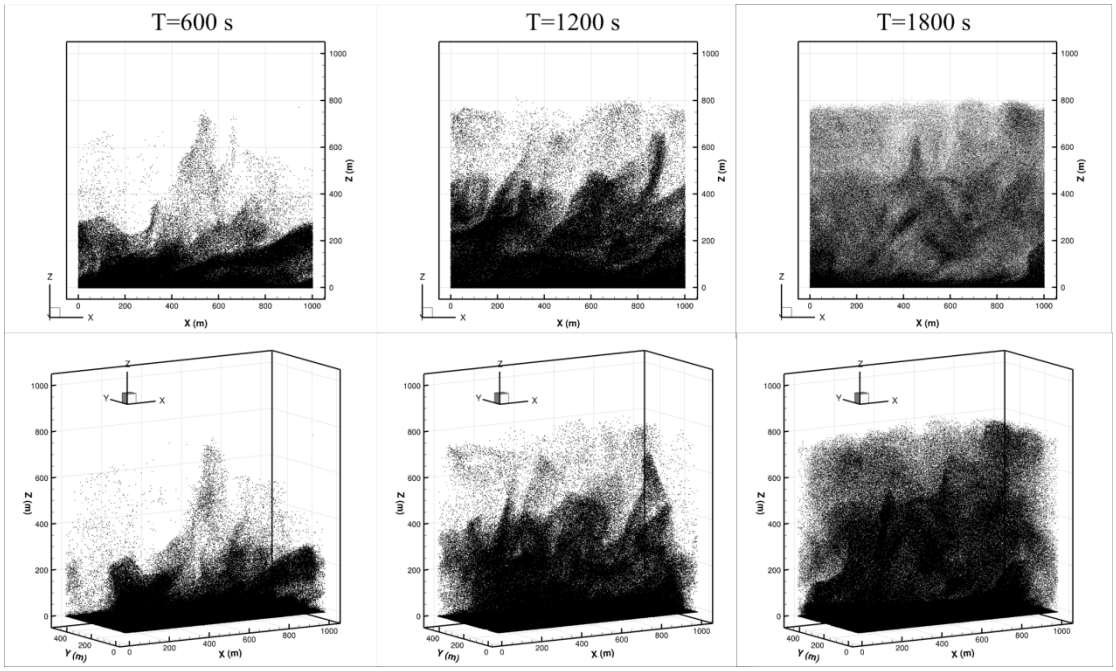


**Figure** 2. Drifting snow storm at different moments under the friction velocity of 0.29 $ms^{-1}$.

When drifting snow occurs in the atmospheric boundary layer, updrafts and turbulence fluctuations can send snow particles to high altitude, forming a fully developed drifting snow storm. Fig. 2 shows the drifting snow storm in the atmospheric boundary layer at different moments, in which the friction velocity is $u_* = 0.29\ ms^{-1}$ and dark spots represent snow particles. It can be seen that drifting snow storm experiences an evolution process from near the surface to high altitudes, which induces the fact that particle concentration decreases along increasing height. The high concentrations of drifting snow cloud are generally below 500 m, though snow particles may reach up to approximately 800 m under this condition. This is also

consistent with observations (Mahesh et al., 2003; Palm et al., 2011).

Since a drifting snow storm exhibits a different structure from bottom to top, the evolution of particle number density profile in the drifting snow storm is shown in Fig. 3, which is also compared with measurements of Mann et al. (2000) . From this figure, the thickness of the drifting snow layer obviously increases with time, and almost approaches its steady state after 1200 s. At the same time, the particle number density basically decreases with height, which is consistent with the measurements of Mann et al. (2000) at various friction velocities. The predicted particle number density at the surface is much larger than at higher altitude and observations, mainly because the saltating particles are also included.

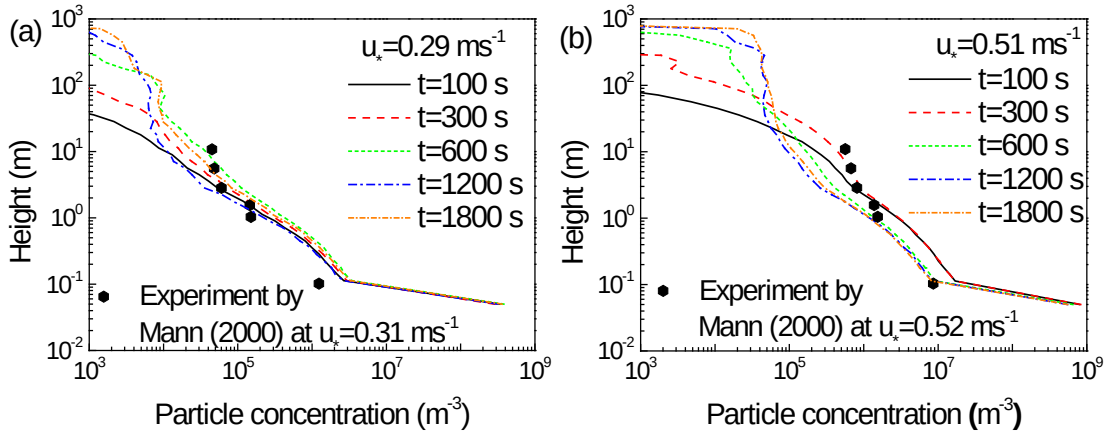


**Figure** 3. Evolution of particle number density under various friction velocities (a) 0.29 $ms^{-1}$ and (b) 0.51 $ms^{-1}$.

Generally, smaller particles are more likely to be transported higher in the air. Fig. 4 shows the variation of modeled average particle diameter versus height, which is also compared with various field measurements (Nishimura and Nemoto, 2005; Schmidt, 1982). Similar to the field observations, the average particle size basically decreases with height at lower altitude but is almost constant above 1 m. The average

261 particle diameter is approximately 75 μm ranging from one meter to hundreds of
262 meters in height, which is also consistent with the measurements of K Nishimura and
263 Nemoto (2005).

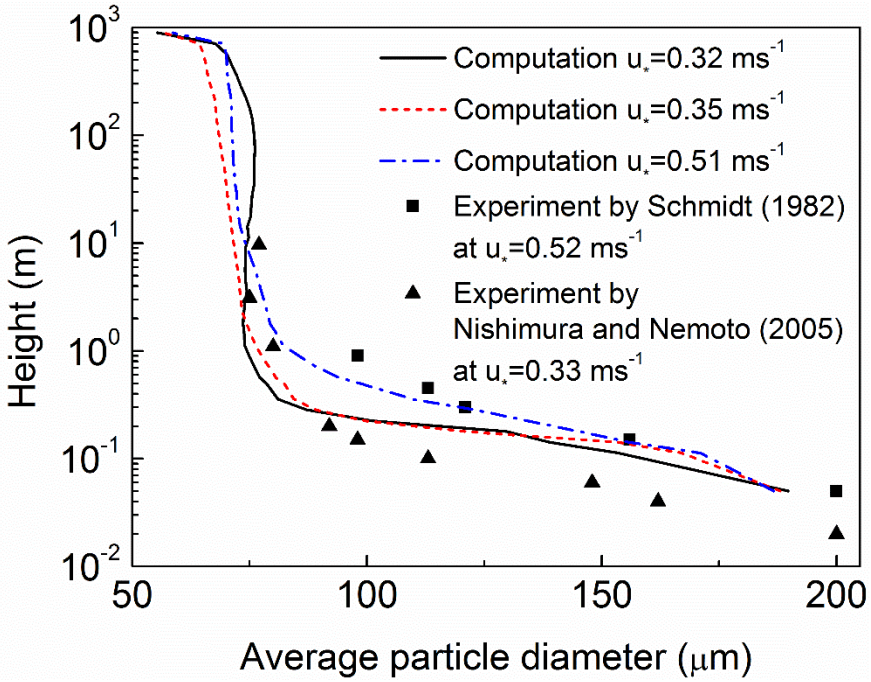


264

265 **Figure** 4. Variation of average particle diameter versus height.

266 Then, the particle size distributions at various heights are also compared with
267 experiment results. As shown in Fig. 5, the heights are 0.05 m, 0.5 m and 1 m. The
268 modeled particle size distributions at various heights are consistent with the
269 measurements (Nishimura and Nemoto, 2005; Schmidt, 1982). Therefore, the
270 established model is able to produce a large-scale drifting snow storm.

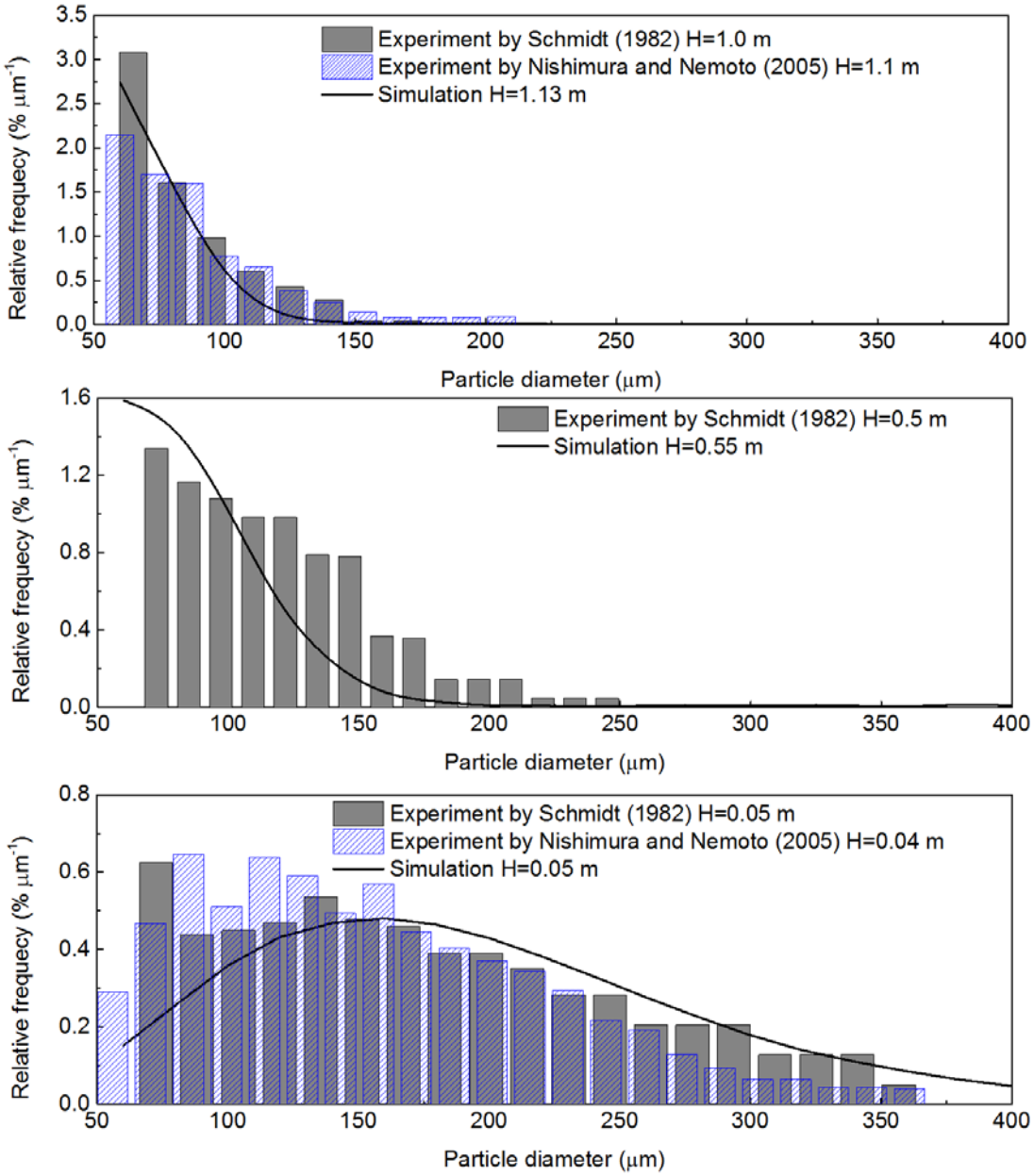


**Figure** 5. Particle size distribution at various heights.

Besides, it can be seen that the proportion of particles below 100 μm in diameter at 0.05 m is smaller than that of the experimental result. The reason could be that mid-air collisions, occurred frequently within the high concentration saltating snow cloud at the near surface, play an important role in conveying larger particles to higher altitude(Carneiro et al., 2013). However, the mid-air collision mechanism is beyond the scope of the current study.

### 3.2 Snow transport flux

The snow transport flux is of great importance to predict the mass and energy balances of ice sheets. The total transport flux can be obtained from vertical integration of the snow transport flux profile.

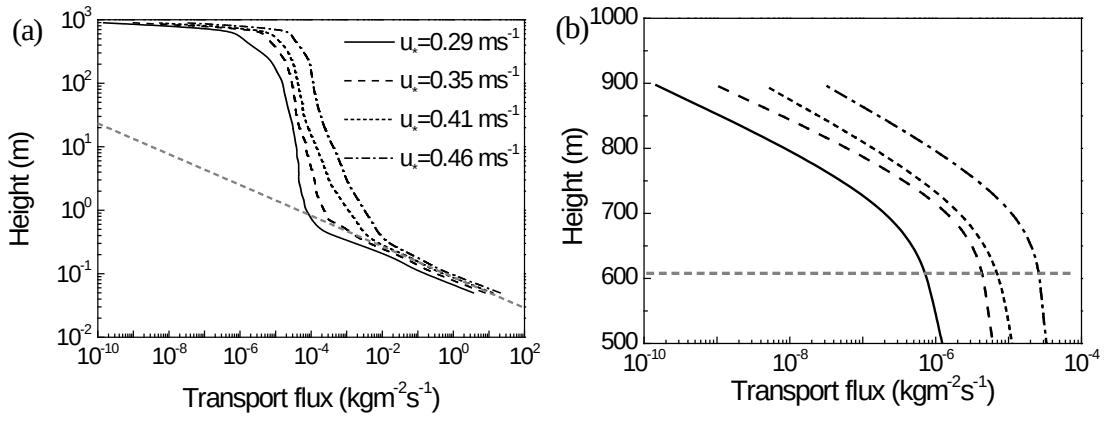


**Figure** 6. Variations of snow transport flux versus height.

The profiles of snow transport rate, per unit area, per unit time, under various friction velocities are shown in Fig. 6(a). It can be seen that the transport flux undergoes a sharp decrease with height at lower altitude (e.g., below 1.0 m), however, the transport flux tends to decrease rather gentle until almost the top of the drifting snow storm, as shown in Fig. 6(b), probably due to the large-scale turbulent motion and increasing wind speed with height. In other words, the suspension flux of drifting snow at higher altitudes, previously not observed, may be much larger than we previously thought. The mean horizontal wind speed profiles of the fully developed turbulent boundary layer under various friction velocities are shown in Fig. 7. The horizontal wind speed increases with height and changes into a constant above the boundary layer. The rapid decrease of the snow transport flux occurs at about the top of the turbulent boundary layer, mainly because turbulences become weaker above

this height and less particles can be transported to a higher altitude.

Besides, the transition of snow transport flux profile at about 1 m should be mainly caused by the different motion states of particles with different particle sizes, as shown in Fig. 4. Above the critical height, particles generally follow the turbulent flow in the state of suspension because their gravities and relaxation times are small enough. However, plenty of larger particles at the near surface make the particles velocity differs from the wind speed, since particle inertia plays an important role.

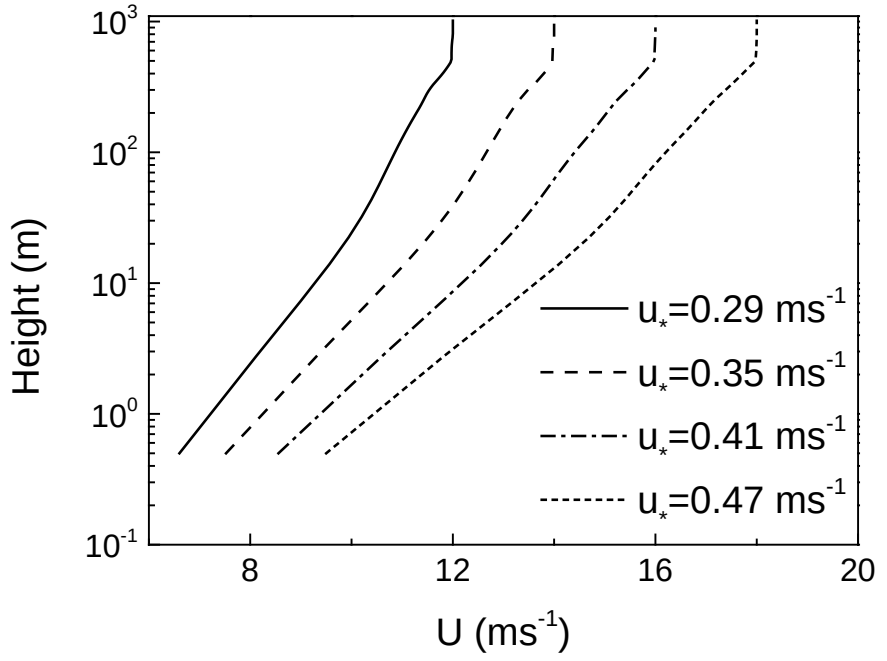


**Figure** 7. Horizontal wind speed profiles of the fully developed turbulent boundary layer under various friction velocities.

In previous studies, only the transport fluxes at the near surface are ~~profile is~~ commonly ~~described using an exponential decay form based on the extrapolation from measurements~~ measured~~near the surface~~ (Mann et al., 2000; Nishimura and Nemoto, 2005; Schmidt, 1982; 1984; Tabler, 1990), thus, the features of the entire transport flux profile is largely unclear, which may result in ~~a~~ considerable

uncertainties ~~underestimate of~~ about the total transport flux. The proportions of suspension flux above a given height $h_c$ (referred as $Q_c$) to the total suspension flux $Q_s$ are shown in Fig. 7, in which snow particles below 0.1 m are not calculated (Mann et al., 2000).

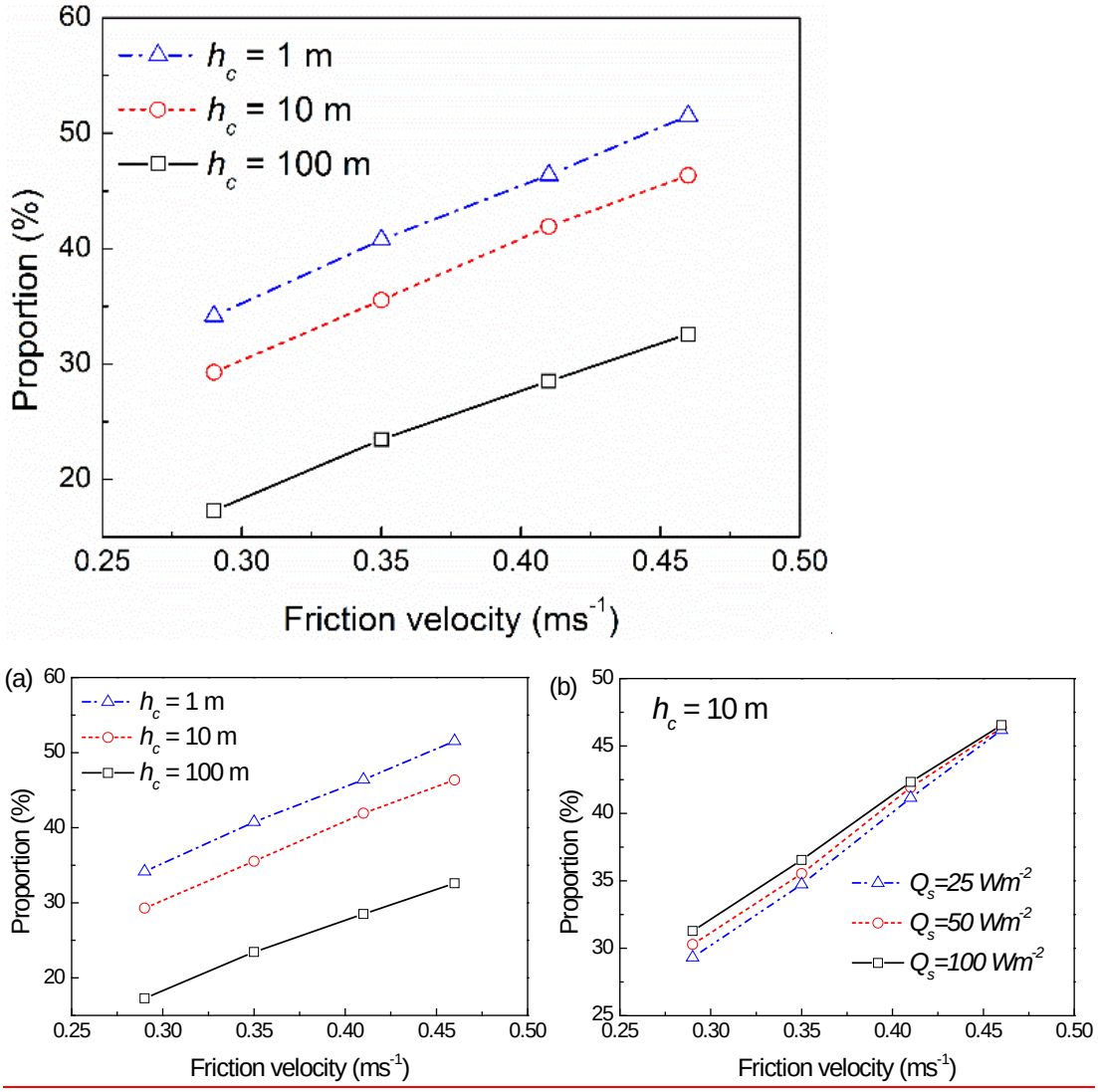


**Figure** ~~7~~8. Proportion of suspension flux above $h_c$ to the total suspension flux under (a) various friction velocities and (b) various surface heat fluxes $Q_s$.

From Fig. ~~7~~8 (a), the contribution of $Q_c$ to the total suspension flux is non-negligible under various $h_c$, the proportion of $Q_c$ when $h_c$ =100 m to the total suspension flux has exceeded 30% when the friction velocity is 0.46 ms$^{-1}$. At the same

time, the proportion of $Q_c$ to the total suspension flux increases with friction velocity but decreases with increasing $h_c$. From Fig. 8 (b), it can be seen that the proportion $Q_c$ to the total suspension flux is only slightly affected by the surface heat flux, which indicates that the structures of drifting snow storm are not sensitive to the surface heat flux under this condition. The influence of surface heat flux is also weakened by the increasing friction velocity, mainly because larger friction velocity results in stronger turbulence under the actions of wind shear.

In this way, not only the snow transport flux, but also the sublimation of suspended snow particles should be reevaluated because the sublimation rate of snow particles higher in the air may be much larger than near the surface due to the lower air humidity and greater wind speed at higher altitude (Mann et al., 2000; Nishimura and Nemoto, 2005; Schmidt, 1982; 1984; Tabler, 1990).

### 3.3 Structures in a drifting snow storm

In a drifting snow storm, particles aggregate locally and produce special spatial structures (as shown in Fig. 2). These structures should be directly related to the turbulence structures present in the atmospheric boundary layer. Drifting snow storms without atmospheric turbulence are shown in Fig. 8. This simulation is achieved by replacing the resolved wind speed at particle's position ($\tilde{u}_i\left(\vec{x}_p\right)$) with a given value obtained from the standard logarithmic profile, and the other model settings and simulation procedures stay the same with other simulations. In this way, the effect of large-scale turbulent structures on the development of the drifting snow storm vanishes. Compared with Fig. 2, drifting snow particles mainly travel at the near

surface with a uniform spatial distribution when atmospheric turbulence is not included.

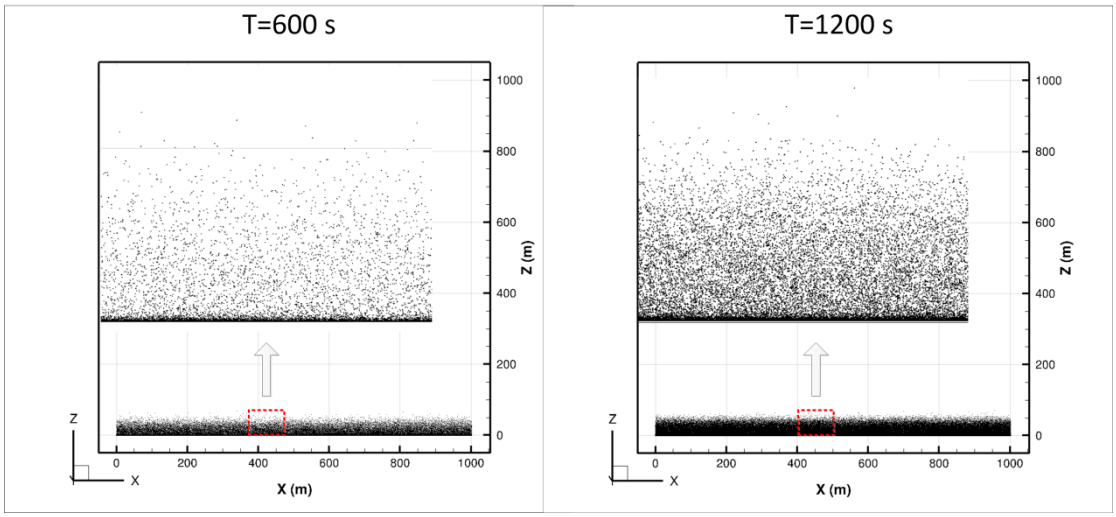


**Figure** 8. Drifting snow storm without atmospheric turbulence under friction velocity of 0.35 $ms^{-1}$.

It is known that snow particles will become suspended if the local vertical wind speed exceeds the terminal velocity of particle. In a turbulent atmospheric boundary layer, there exists a large amount of turbulent structures with different scales and shapes. The vertical wind speed component of large-scale turbulence (namely, updraft) plays an important role in carrying snow particles to high altitude, while small scale turbulence (e.g., the SGS fluctuating velocity) tends to spread particles from high concentration zones to low concentration zones. As shown in Fig. 9(a), at the initial period of a drifting snow storm, the structures in the drifting snow storm are consistent with large-scale updrafts, and snow particles are mainly located in the updraft. With the further development of the drifting snow storm, as shown in Fig. 9(b), more snow particles are scattered around the updraft bubbles although high concentration particle clouds are still in the wind bubbles. When drifting snow storm

approaches its saturated state, snow particle clouds are almost connected together with numerous high concentration zones inside.

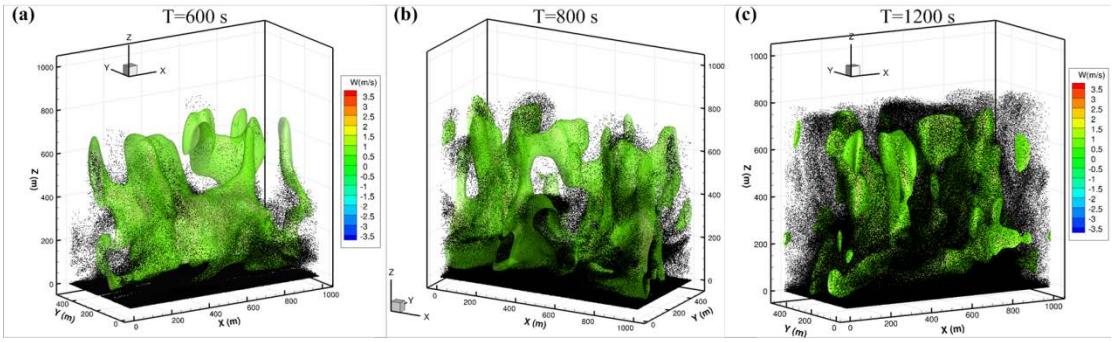


**Figure** 9. Evolution of drifting snow storm and vertical wind speed bubbles under friction velocity of 0.35 $ms^{-1}$, and wind bubbles are iso-surface of vertical wind speed with a value of 1.0 $ms^{-1}$ (corresponding to the critical wind speed at which the particle of mean particle size becomes suspended particle, since the maximum diameter of suspended particles is found to be approximately equals to the mean particle size of the lift-off particles).

The evolution of the depth of drifting snow storm can be divided into three typical stages. In sequence, these phases are the rapid growth phase, the gentle growth stage, and an equilibrium state, as shown in Fig. 10. Here, the depth of drifting snow storm refers to the average height of the topmost particle during this period (100 s). The rapid growth stage is mainly driven by large-scale turbulent motion, while the turbulent diffusion by the SGS fluctuating velocity is the main contributor to the gentle growth stage. The duration of second stage decreases with increasing friction velocity, which mainly comes from the stronger turbulent diffusion under larger friction velocities.

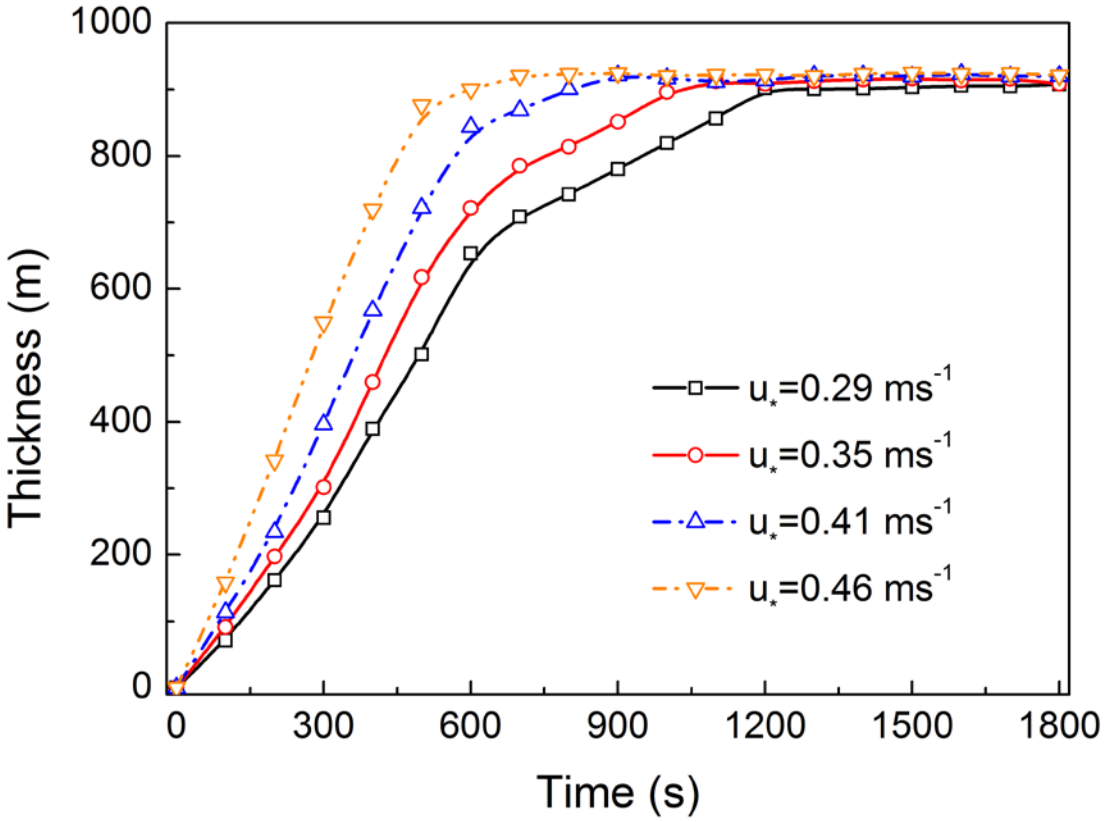


**Figure** 10. Time evolutions of the thickness of drifting snow storm under various friction velocities.

At the same time, the time required for the drifting snow storm to reach its maximum thickness decreases with friction velocity, ranging from about 1200 s to approximate 600 s when the friction velocity increases from 0.29 $ms^{-1}$ to 0.46 $ms^{-1}$. The thicknesses of saturated drifting snow storms ~~is~~ are almost constant with a value approximately 900 m under different friction velocities, probably because the boundary layer depth as well as the surface heat flux are unchanged. Higher domain heights are also tested with the same model settings, and the thickness of the drifting snow seems basically unchanged. Drifting snow storm with difference thicknesses may be achieved by changing the initial state of the air and surface heat flux. Thus, the final thickness of a drifting snow storm should be largely dependent on the

maximum height of atmospheric turbulences.

## 4 Conclusion

In this work, large-scale drifting snow storms are simulated in a large eddy simulation combined with a particle tracking model that includes subgrid scale velocity fluctuations. A typical drifting snow storm of several hundred meters in depth is generated, and the structure of the particle cloud with different concentrations is also produced. The transport flux profile has obviously different slopes near the surface compared to higher altitudes, that is, transport flux at near surface decreases with height sharply, but decreases more gentle at higher altitude. Previous studies may largely underestimate the total transport during drifting snow storms.

At the same time, the evolution of the thickness of drifting snow storm generally contains three stages. Drifting snow storm development generally begins with a rapid growth stage driven by the large scale atmospheric turbulent motions, followed by a gentle growth stage driven by the SGS fluctuating wind speed, before reaching an equilibrium stage when the drifting snow approaches a saturated state. The second stage becomes shorter with increasing friction velocity, mainly because stronger turbulence under higher friction velocity enhances the turbulent diffusion of particles.

*Acknowledgements.* This work is supported by the CARDC Fundamental and Frontier Technology Research Fund (FFTRF-2017-08, FFTRF-2017-09), the State Key Program of National Natural Science Foundation of China (91325203), the National Natural Science Foundation of China (11172118, 41371034), and the Innovative

Research Groups of the National Natural Science Foundation of China (11121202), National Key Technologies R & D Program of China (2013BAC07B01).

**References:**

Bintanja, R.: Snowdrift suspension and atmospheric turbulence. Part I: Theoretical background and model description, Boundary-Layer Meteorology, 95, 343-368, 2000.

Bintanja, R.: Characteristics of snowdrift over a bare ice surface in Antarctica, Journal of Geophysical Research Atmospheres, 106, 9653-9659, 2001.

Budd, W. F.: The Byrd snow drift project : outline and basic results, 71-134, American Geophysical Union, Washington, DC, 1966.

Carneiro, M. V., Araújo, N. A., Pähtz, T., and Herrmann, H. J.: Midair collisions enhance saltation, Phys.rev.lett, 111, 058001, 2013.

Cess, R. D., and Yagai, I.: Interpretation of Snow-Climate Feedback as Produced by 17 General Circulation Models, Science, 253, 888-892, 1991.

Chang, A. T. C., Foster, J. L., and Hall, D. K.: Nimbus-7 SMMR Derived Global Snow Cover Parameters, Annals of Glaciology, 9, 39-44, 2016.

Clift, R., Grace, J. R., and Weber, M. E.: Bubbles, drops, and particles, 263-264, 1978.

Clifton, A., Rüedi, J. D., and Lehning, M.: Snow saltation threshold measurements in a drifting-snow wind tunnel, Journal of Glaciology, 52, 585-596, 2006.

Déry, S. J., and Yau, M. K.: A Bulk Blowing Snow Model, Boundary-Layer Meteorology, 93, 237-251, 1999.

Deardorff, J. W.: Stratocumulus-capped mixed layers derived from a three-dimensional model, Boundary-Layer Meteorology, 18, 495-527, 1980.

Dingle, W. R. J., and Radok, U.: Antarctic snow drift and mass transport, Int. Assoc. Sci. Hydrol. Publ., 55, 77-81, 1961.

Doorschot, J. J. J., Lehning, M., and Vrouwe, A.: Field measurements of snow-drift threshold and mass fluxes, and related model simulations, Boundary-Layer Meteorology, 113, 347-368, 2004.

Dupont, S., Bergametti, G., Marticorena, B., and Simoëns, S.: Modeling saltation intermittency, Journal of Geophysical Research Atmospheres, 118, 7109-7128, 2013.

Gallée, H., Trouvilliez, A., Agosta, C., Genthon, C., Favier, V., and Naaim-Bouvet, F.: Transport of Snow by the Wind: A Comparison Between Observations in Adélie Land, Antarctica, and Simulations Made with the Regional Climate Model MAR, Boundary-Layer Meteorology, 146, 133-147, 2013.

Gordon, M., and Taylor, P. A.: Measurements of blowing snow, Part I: Particle shape, size distribution, velocity, and number flux at Churchill, Manitoba, Canada, Cold Regions Science & Technology, 55, 63-74, 2009.

Guyomarch, G., Goetz, D., Vionnet, V., Naaimbouvet, F., and Deschatres, M.: Observation of Blowing Snow Events and Associated Avalanche Occurrences,

2014.
Hanesiak, J. M., and Wang, X. L.: Adverse-Weather Trends in the Canadian Arctic, Journal of Climate, 18, 3140-3156, 2005.
Hinzman, L. D., Bettez, N. D., Bolton, W. R., Chapin, F. S., Dyurgerov, M. B., Fastie, C. L., Griffith, B., Hollister, R. D., Hope, A., and Huntington, H. P.: Evidence and Implications of Recent Climate Change in Northern Alaska and Other Arctic Regions, Climatic Change, 72, 251-298, 2005.
Huang, N., Dai, X., and Zhang, J.: The impacts of moisture transport on drifting snow sublimation in the saltation layer, Atmospheric Chemistry & Physics, 16, 7523-7529, 2016.
Huang, N., and Shi, G.: The significance of vertical moisture diffusion on drifting Snow sublimation near snow surface, Cryosphere, 11, 3011-3021, 2017.
Huang, N., and Wang, Z. S.: A 3-D simulation of drifting snow in the turbulent boundary layer, Cryosphere Discussions, 9, 301-331, 2015.
Huang, N., and Wang, Z. S.: The formation of snow streamers in the turbulent atmosphere boundary layer, Aeolian Research, 23, 1-10, 2016.
King, J. C.: Some measurements of turbulence over an antarctic ice shelf, Quarterly Journal of the Royal Meteorological Society, 116, 379-400, 1990.
Kobayashi, S.: Snow Transport by Katabatic Winds in Mizuho Camp Area, East Antarctica, Journal of the Meteorological Society of Japan, 56, 130-139, 1978.
Lehning, M., Löwe, H., Ryser, M., and Raderschall, N.: Inhomogeneous precipitation distribution and snow transport in steep terrain, Water Resources Research, 44, 278-284, 2008.
Lenaerts, J. T. M., and Broeke, M. R. V. D.: Modeling drifting snow in Antarctica with a regional climate model: 2. Results, Journal of Geophysical Research Atmospheres, 117, D05109, 2012.
Li, L., and Pomeroy, J. W.: Estimates of Threshold Wind Speeds for Snow Transport Using Meteorological Data, Journal of Applied Meteorology, 36, 205-213, 1997.
Mahesh, A., Eager, R., Campbell, J. R., and Spinhirne, J. D.: Observations of blowing snow at the South Pole, Journal of Geophysical Research Atmospheres, 108, 4707, 2003.
Mann, G. W., Anderson, P. S., and Mobbs, S. D.: Profile measurements of blowing snow at Halley, Antarctica, Journal of Geophysical Research Atmospheres, 105, 24491-24508, 2000.
Meneveau, C., Lund, T. S., and Cabot, W. H.: A Lagrangian dynamic subgrid-scale model of turbulence, Journal of Fluid Mechanics, 319, 353-385, 1996.
Moeng, C. H., and Sullivan, P. P.: A Comparison of Shear- and Buoyancy-Driven Planetary Boundary Layer Flows, Journal of the Atmospheric Sciences, 51, 999-1022, 1994.
Mohamed, N., Florence, N. B., and Hugo, M.: Numerical simulation of drifting snow: erosion and deposition models, Annals of Glaciology, 26, 191-196, 1998.
Nemoto, M., and Nishimura, K.: Numerical simulation of snow saltation and suspension in a turbulent boundary layer, Journal of Geophysical Research Atmospheres, 109, D18206, 2004.

Nishimura, K., and Nemoto, M.: Blowing snow at Mizuho station, Antarctica, Philosophical Transactions, 363, 1647, 2005.
Nishimura, K., Yokoyama, C., Ito, Y., Nemoto, M., Naaim‐Bouvet, F., Bellot, H., and Fujita, K.: Snow particle speeds in drifting snow, Journal of Geophysical Research Atmospheres, 119, 9901-9913, 2015.
Palm, S. P., Yang, Y., Spinhirne, J. D., and Marshak, A.: Satellite remote sensing of blowing snow properties over Antarctica, Journal of Geophysical Research Atmospheres, 116, D16123, 2011.
Pomeroy, J. W., and Essery, R. L. H.: Turbulent fluxes during blowing snow: field tests of model sublimation predictions, Hydrological Processes, 13, 2963-2975, 1999.
Pomeroy, J. W., and Gray, D. M.: Saltation of snow, Water Resources Research, 26, 1583–1594, 1990.
Sbuhei, T.: Characteristics of Drifting Snow at Mizuho Station, Antarctica, Annals of Glaciology, 6, 71-75, 1985.
Schmidt, R. A.: Vertical profiles of wind speed, snow concentration, and humidity in blowing snow, Boundary-Layer Meteorology, 23, 223-246, 1982.
Schmidt, R. A.: Transport rate of drifting snow and the mean wind speed profile, Boundary-Layer Meteorology, 34, 213-241, 1984.
Schneiderbauer, S., and Prokop, A.: The atmospheric snow-transport model: SnowDrift3D, Journal of Glaciology, 57, 526-542, 2011.
Smagorinsky, J.: GENERAL CIRCULATION EXPERIMENTS WITH THE PRIMITIVE EQUATIONS, Monthly Weather Review, 91, 99-164, 1963.
Sturm, M., and Stuefer, S.: Wind-blown flux rates derived from drifts at arctic snow fences, Journal of Glaciology, 59, 21-34, 2013.
Sugiura, K., and Maeno, N.: Wind-Tunnel Measurements Of Restitution Coefficients And Ejection Number Of Snow Particles In Drifting Snow: Determination Of Splash Functions, Boundary-Layer Meteorology, 95, 123-143, 2000.
Tabler, R. D.: Estimating snow transport from wind speed record : Estimates versus measurements at Prudhoe Bay, paper presented at Alaska, Meeting of Western Snow Conference, 1990.
Uematsu, T., Nakata, T., Takeuchi, K., Arisawa, Y., and Kaneda, Y.: Three-dimensional numerical simulation of snowdrift, Cold Reg.sci.technol, 20, 65-73, 1991.
Vinkovic, I., Aguirre, C., Ayrault, M., and Simoëns, S.: Large-eddy Simulation of the Dispersion of Solid Particles in a Turbulent Boundary Layer, Boundary-Layer Meteorology, 121, 283-311, 2006.
Vionnet, V., Martin, E., Masson, V., Guyomarc'H, G., Naaimbouvet, F., Prokop, A., Durand, Y., and Lac, C.: Simulation of wind-induced snow transport in alpine terrain using a fully coupled snowpack/atmosphere model, Cryosphere Discussions, 7, 2191-2245, 2013.
Xue, M., Droegemeier, K. K., Wong, V., Shapiro, A., Brewster, K., Carr, F., Weber, D., Liu, Y., and Wang, D.: The Advanced Regional Prediction System (ARPS) – A multi-scale nonhydrostatic atmospheric simulation and prediction tool. Part II:

Model physics and applications, Meteorology & Atmospheric Physics, 76, 143-165, 2001.
Zhang, J., and Huang, N.: Simulation of Snow Drift and the Effects of Snow Particles on Wind, Modelling & Simulation in Engineering, 2008, 408075, 2008.
Zwaaftink, C. D. G., Diebold, M., Horender, S., Overney, J., Lieberherr, G., Parlange, M. B., and Lehning, M.: Modelling Small-Scale Drifting Snow with a Lagrangian Stochastic Model Based on Large-Eddy Simulations, Boundary-Layer Meteorology, 153, 117-139, 2014.